

PRELIMINARY RESULTS ON THE INCLUSIVE  
ELECTROPRODUCTION OF HADRONS\*

J. T. Dakin, G. J. Feldman, W. L. Lakin\*\*,  
F. Martin, M. L. Perl, E. W. Petraske†, W. T. Toner††  
Stanford Linear Accelerator Center  
Stanford University, Stanford, California 94305

ABSTRACT

The electroproduction of hadrons was studied with a wide-aperture spectrometer. Preliminary data are presented for the electron-scattering region  $-0.5 > q^2 > -2.5$  (GeV/c)<sup>2</sup>,  $4 < \nu < 14$  GeV. Distributions of the electroproduced hadrons in the 3 inclusive variables  $\varphi$ ,  $p_{\perp}^2$  and  $x$  are studied in the region  $x > 0$ . No significant azimuthal dependence is seen in the data. The  $p_{\perp}^2$  distributions are similar to that of photoproduction, but perhaps somewhat broader. They do not appear to depend on  $q^2$ ,  $\nu$ , or  $x$  within statistics. The  $x$  distributions are similar to those from photoproduction, but the negative hadron distribution drops more sharply with  $x$ . A striking difference from photoproduction is observed in the excess of positive to negative hadrons at high  $x$  and high  $q^2$ . A mass plot of elastically electroproduced rho mesons is presented.

(Submitted to the XVI International Conference on High Energy Physics, Batavia, Illinois, Sept. 6-13, 1972. A shorter version of this paper was submitted to Phys. Rev. Letters.)

- 
- \* Work supported by the U. S. Atomic Energy Commission.  
\*\* Present address: Birmingham Radiation Centre, University of Birmingham, P.O. Box 363, Birmingham B15 2TT, England.  
† Present address: Vanderbilt University, Nashville, Tennessee 37203.  
†† Present address: Rutherford High Energy Laboratory, Chilton, Didcot, Berkshire, England.

## I. Introduction

With the recent work in deep inelastic electron-nucleon scattering and its subsequent theoretical interpretations, there has been increasing interest in the hadronic final states produced in such interactions.<sup>1</sup> Here we report some preliminary results on the inclusive electroproduction of hadrons.

In this experiment, we detected in coincidence an electron scattered from a hydrogen target and one or more electroproduced hadrons. Taking each combination of a scattered electron and an electroproduced hadron as an independent inclusive event, the cross section is a function of six variables. Three of them are determined by the electron system:  $E$ , the incident electron energy in the laboratory (fixed at 19.5 GeV for all of our data);  $q^2$ , the invariant momentum transfer squared to the scattered electron; and  $\nu$ , the electron energy loss in the laboratory. The remaining three, which concern the detected hadron, are calculated relative to the direction of the electron three-momentum transfer:  $x$ , the ratio of the longitudinal momentum in the virtual photoproduction center of mass system to the maximum possible;  $p_{\perp}^2$ , the transverse momentum squared; and  $\varphi$ , the hadron aximuthal angle.

Virtual photoproduction cross sections can be derived from experimental cross sections by

$$\frac{d\sigma}{dq^2 d\nu d^3 p_{\text{had}}} = \Gamma(E, q^2, \nu) \frac{d\sigma_{\gamma}^*(q^2, \nu)}{d^3 p_{\text{had}}} \quad (1)$$

where the  $\Gamma$  function contains the electrodynamic factors describing the electron-photon vertex. We will report here ratios of differential virtual photon cross sections to the total virtual photon cross section. These ratios are derived directly from our data since we had no requirement for a hadron in our trigger.

The differential cross sections will be given in a Lorentz invariant form:

$$E \frac{d\sigma(q^2, \nu)}{d^3p} = 2 \frac{E^*}{p_{\max}^*} \frac{d\sigma(q^2, \nu)}{dx dp^2 d\varphi}, \quad (2)$$

where  $E^*$  is the energy of the hadron in the center of mass and  $p_{\max}^*$  is the maximum possible center of mass momentum.

## II. Apparatus

The experimental apparatus consisted of a 19.5 GeV electron beam incident on a target, and a large aperture spectrometer to detect a large fraction of the forward final state particles with lab momenta greater than  $\sim 1$  GeV/c. These elements are shown in Fig. 1, and discussed in greater detail below.

The electron beam contained typically  $10^4 e^-$  per 1.5  $\mu$ sec long SLAC pulse. At the experimental target, the beam had an rms width of  $0.5 \text{ mm} \times 0.5 \text{ mm}$ , and an rms divergence less than  $0.2 \text{ mrad} \times 0.2 \text{ mrad}$ . There the beam was very well collimated, with fewer than  $1 e^-$  in  $10^5$  outside a 0.5 cm diameter circle. The momentum band was 0.2% at 19.5 GeV/c.

The target was 4 cm long, and was filled with either hydrogen or deuterium. Only the hydrogen data is reported here.

The spectrometer magnet had 1.37 m diameter pole faces separated by 0.91 m. It was centered on the beam line, 2.54 m downstream from the target, with its principal field component horizontal. At the magnet center, this field was 10 k Gauss, and the field integral 17 k Gauss-meters.

The unscattered beam and the forward electromagnetic backgrounds passed through the magnet in a field-free region created by a cylindrical superconducting tube.<sup>2</sup> Beyond the magnet were two optical spark chambers separated by 1.7 m. The chambers had inactive holes through their centers, where the beam

tube passed. The apertures of the magnet, spark chambers, and beam tube produced the acceptance shown in Fig. 2

The apparatus was triggered on the detection of a scattered electron by a hodoscope of 20 scintillation counters and 11 shower counters<sup>3</sup> behind the second spark chamber. The shower counter thresholds were set to  $\sim 5$  GeV. Photon triggers were eliminated by the requirement that a shower counter fire coincident with the scintillators in front of it. The kinematic range of inelastic electron scatters covered by this trigger was roughly  $|q^2| > 0.3(\text{GeV}/c)^2$ ,  $\nu < 15$  GeV. There was no hadron requirement in the trigger.

For each trigger a single picture was taken of the optical spark chambers on 70 mm film. The camera was located in the horizontal plane 21.6 m from the beam line with its optic axis aligned perpendicular to the beam. Each picture contained four views of each chamber, a direct view, a top and a bottom view in small angle stereo, and a rear view to expose tracks blocked in the direct view by a beam pipe. Figure 3 contains a picture of an event which contains a candidate for an elastically produced rho meson.

A PDP-8 computer recorded scintillation and shower counter status, shower counter pulse heights, and scintillation counter timing information for each event.

The beam flux was integrated by a quantameter located behind the shower counters and was monitored instantaneously by a surface-barrier detector.<sup>4</sup>

### III. Data Collection and Reduction

During the experiment we recorded 250,000 pictures with the H<sub>2</sub> target and 110,000 with D<sub>2</sub>. These data samples contained  $2.6 \times 10^{12}$  and  $0.7 \times 10^{12}$  incident electrons respectively. Here we report a preliminary analysis of the H<sub>2</sub> data.

The pictures were scanned and measured and the particle trajectories were reconstructed in space using two independent systems. The first was Hummingbird II, a flying spot digitizer, with which we measured all tracks in all 250,000 pictures.<sup>5</sup> The second was a conventional hand system with which we measured only events with 2 or more tracks out of a reduced sample of 50,000 pictures. For the latter system, 2-track candidate pictures were pre-selected with high (>99%) efficiency by Hummingbird.

Each system had only ~50% efficiency for fully reconstructing events with 2 or more tracks, largely because of confusion introduced by spurious tracks. We have not as yet thoroughly studied biases introduced by these inefficiencies. Biases, if any, should be different for the two systems since the Hummingbird identifies tracks on the basis of the stereo reconstruction while the hand system relies on pattern recognition of spark densities. We have verified that both systems give the same physics results within statistics, and that the spatial agreement between those tracks which both systems reconstruct is better than 0.5 mm rms. The data reported here are solely from the Hummingbird system. The hand data have only been used as an internal check.

The momentum of each reconstructed track was computed by propagating the track back through the magnet, and adjusting the momentum until the track intercepted the target vertically. Tracks which did not, then, strike the target horizontally were thrown out. The rms momentum resolution was 2% at 10 GeV.

In each reconstructed picture, the electron was identified by matching the positions and momenta of tracks to the position and pulse height of the shower counter which triggered the event. In the Hummingbird data, electrons were identified in 33% of the frames. The remaining tracks which were consistent

with the scintillator hodoscope pattern for an event were assumed to be hadrons. In a picture in which an electron was identified, if a hadron was present it was identified with  $(70 \pm 10\%)$  efficiency.

We have no means of distinguishing pions, kaons, and protons from each other. Hence we will refer only to positively and negatively charged hadrons and use the symbol "h" to describe them.

Each electron-hadron pair was analyzed as an inclusive event. The virtual photon parameters ( $q^2$ ,  $\nu$ ), and the hadron inclusive parameters ( $\varphi$ ,  $p_{\perp}^2$ ,  $x$ , charge) were calculated. To prepare the physics distributions each event was weighted inversely as its detection probability, a function of all six of the above variables. To study the dependence of the data on one of these variables, we summed over some range of the other five variables. When such summations passed over small regions of zero acceptance, corrections were made for the missing events.

The cross sections thus obtained were normalized to the total virtual photo-production cross section in the same  $q^2$ ,  $\nu$  region ( $\sigma(q^2, \nu)$ ), obtained from the data. The data presented here are 6244 events from the region  $4 < \nu < 14$  GeV,  $-0.5 < q^2 < -2.5$  (GeV/c) $^2$ , the region where the virtual photon direction is well within the geometric acceptance. Unless otherwise stated, the data are summed over this entire region.

We studied the zero order radiative effects by assuming that, in addition to the material that was actually present, there was  $(3/4) \cdot (\alpha/\pi) \cdot [\ln(-q^2/m^2)-1]$  radiation lengths of material before and after the interaction.<sup>6</sup> Data were simulated in which the incident and scattered electrons underwent random bremsstrahlung.

This radiative degradation produced no noticeable effect in the shapes of the  $p_{\perp}^2$  and  $x$  distributions at the statistical level of this experiment. No corrections for radiative effects have been made in the data presented here. The simulation indicated that spatial resolution effects are also negligible.

The errors given in figures and tables in this report represent statistical errors only. There is in addition a possible 15% error due primarily to uncertainty in the level of Hummingbird efficiency.

#### IV. Azimuthal Angle

With the assumption of one-photon exchange, the azimuthal angle ( $\varphi$ ) dependence must be of the form

$$\frac{d\sigma}{d\varphi} = A + \epsilon B \cos 2\varphi + \sqrt{\epsilon(1+\epsilon)} C \cos \varphi \quad (3)$$

where  $\epsilon$  is the transverse polarization of the virtual photon. The phase of  $\varphi$  is such that the incident electron is at  $\varphi = 0$ . For the data presented here the average polarization was 83%. The term proportional to  $\cos(2\varphi)$  is due to transverse polarization of the photon and is present in  $\pi^-$  photoproduction at high  $x$  at the 30% level.<sup>7</sup> The term proportional to  $\cos \varphi$  is due to interference between transverse and longitudinal photons and is unique to electroproduction.

The hadron azimuthal angle dependence of the data was studied for 2 different  $x$  ranges, and for positive and negative hadrons (see Fig. 4). We see no significant  $\varphi$  dependence in the data, although the negative hadron data are consistent with the photoproduction results. As an aid in extracting  $p_{\perp}^2$  and  $x$  distributions, discussed later, we assume that the  $\varphi$  distribution is flat.

#### V. Transverse Momentum Squared

The  $p_{\perp}^2$  dependence of the cross section is shown for the entire  $q^2$  range (Fig. 5), and for 4 smaller  $q^2$  ranges (Figs. 6, 7). Exponential fits with the

formula  $Ae^{-bp_{\perp}^2}$  have been done, and the slope parameters ( $b$ ) are presented in Fig. 8.

The  $p_{\perp}^2$  dependence is seen to be independent of  $q^2$ , and independent of hadron charge at the statistical level of this experiment. All the data are fit well with the exponential, and with a slope parameter of typically  $b \approx 4.7$   $(\text{GeV}/c)^{-2}$ . This slope is, however, less steep than the slope observed in inclusive photoproduction. We have extracted a value of  $b = 5.9 \pm 0.2$   $(\text{GeV}/c)^{-2}$  for the same  $x$  and  $\nu$  ( $E_{\gamma}$ ) range from the  $\pi^{-}$  photoproduction data of Moffeit et al.<sup>7</sup> The slightly less steep slopes observed here are not believed due to radiation or radiative effects; however, we do not think that this difference should be taken to be a significant effect until we have had an opportunity to perform a more exhaustive analysis of the data.

The  $p_{\perp}^2$  dependence of the cross section is similarly independent of  $\nu$ , as is true approximately in photoproduction.<sup>7</sup> No statistically significant  $x$  dependence of the  $p_{\perp}^2$  distribution was evident either.

## VI. Feynman $x$ Variable

The dependence of the invariant cross section on  $x$  is shown in Figs. 9, 10 and 11 for positive and negative hadrons in a number of  $q^2$  regions. The curve for negative hadrons agrees with the analogous photoproduction<sup>7</sup> curve at low  $x$ , but falls a factor of 2 to 3 below it at higher  $x$ . The slow fall of the photoproduction distribution at moderate  $x$  values is due largely to the production of rho mesons. If proportionally fewer rho mesons were electroproduced than photoproduced, one would expect the distribution to fall more sharply.

The relative cross section for positive hadron production is observed to increase with  $|q^2|$  while the negative hadrons stay fixed (see Figs. 10, 11). This effect will be discussed in greater detail in the following section.

## VII. Charge Ratios

Figure 12 shows the ratio of the invariant cross sections for positive hadrons to those for negative hadrons as a function of  $x$ . There is a striking increase in the ratio as  $x$  increases.

There are no published photoproduction data for this ratio. However, from available information we estimate the photoproduction ratio to be  $1.20 \pm 0.10$  throughout this  $x$  range. The SLAC-Berkeley-Tufts bubble chamber data<sup>8</sup> give a ratio between 1.00 and 1.10 in this range. These data exclude two classes of events, one-prong events and visible strange particle production, which together compose  $\sim 15\%$  of the cross section and which predominately yield positive hadrons. The ratio of  $1.20 \pm 0.10$  is also consistent with low  $p_{\perp}^2$  SLAC spectrometer data.<sup>9</sup> Our data appear to approach the photoproduction value as  $x \rightarrow 0$ .

In Fig. 13 we show the charge ratio as a function of  $q^2$  for two ranges of  $x$ . The ratio increases markedly as  $|q^2|$  increases, and appears to approach the photoproduction value as  $q^2 \rightarrow 0$ .

It is not clear whether the effect shown in Fig. 13 is a function of  $q^2$  or  $\omega = -2M\nu/q^2$  (or both). There is some evidence in the data that at fixed  $q^2$  the charge ratio is largest at small  $\omega$ , but we have been unable to establish this on a statistically significant level for all of our data.

We consider these data to be significant and surprising. As  $|q^2|$  increases or as  $\omega$  decreases, by some mechanism, part of the charge of the proton is being projected forward. We note that quark-parton models can yield a charge ratio as large as 8 at small  $\omega$  and large  $x$ .<sup>10</sup>

### VIII. Partial Multiplicities

We define the partial multiplicity to be the integral

$$\frac{1}{\sigma(q^2, \nu)} \int_{x_0}^1 dx \int_0^\infty dp_\perp^2 \frac{d^2\sigma(q^2, \sigma)}{dp_\perp^2 dx}$$

Table I gives partial multiplicities for  $x_0 = 0.2$  as a function of  $q^2$  summed over  $\nu$  and as a function of  $\nu$  summed over  $q^2$ . As a function of  $|q^2|$  the negative hadron multiplicity stays constant within statistics while the positive hadron multiplicity increases. As a function of  $\nu$  the negative hadron multiplicity again stays reasonably constant while the positive hadron multiplicity falls.

### IX. Rho Production

A preliminary search has been made for 3-track events consistent with the reaction



where the proton is not observed. The resolution in the mass-squared of the proton is  $0.3 \text{ GeV}^2$ , sufficient to exclude events with extra unobserved  $\pi$ 's of appreciable energy. The  $\pi^+ \pi^-$  invariant mass of a sample of events consistent with reaction (4) appears in Fig. 14. The presence of the  $\rho$  meson is obvious.

We do not yet have quantitative information on  $\rho$  production.

### X. Conclusion

We must emphasize again that our data are highly preliminary. They may contain biases of which we are presently unaware. However, we think it unlikely that the addition of more reconstructed events or a more refined analysis will change the major conclusions we have drawn. The data we present here will soon be supplemented by our as yet unanalyzed data on elastic  $\rho$  production and by our data from a deuterium target, as well as by additional data from other

laboratories. Thus, in the near future, we hope to have a good picture of the nature of deep inelastic electroproduction.

#### XI. Acknowledgments

We wish to acknowledge the technical support contributed by numerous SLAC groups, particularly the cooperation from Steve St. Lorant and the Low Temperature group, and John Brown and the Data Analysis group.

Conversations with members of the theory group have been beneficial; J. D. Bjorken, Stan Brodsky, Fred Gilman, Jack Gunion and Haim Harari have been particularly helpful.

We are indebted to Ken Moffeit and his colleagues and Dave Sherden and his colleagues for providing us with their photoproduction data prior to publication.

Byron Dieterle and Benson T. Chertok provided valuable assistance in the early stages of the experiment.

## REFERENCES

1. The current status of these topics is summarized in talks by H. Kendall, K. Berkelman and J. Bjorken in International Symposium On Electron and Photon Interactions at High Energies, Cornell University, Ithaca, N. Y., (1971), edited by N. B. Mistry.
2. F. Martin, S. J. St. Lorant and W. T. Toner, Nucl. Instr. and Methods (to be published).
3. W. L. Lakin, E. W. Petraske, W. T. Toner, Nucl. Instr. and Methods (to be published).
4. W. L. Lakin, R. E. Baggs, Nucl. Instr. and Methods (to be published).
5. J. L. Brown, Stanford Linear Accelerator Center Report No. SLAC-PUB-752 (1970).
6. L. W. Mo and Y. S. Tsai, Rev. Mod. Phys. 41, 205 (1969).
7. K. C. Moffiet, J. Ballam, G. B. Chadwick, M. Della-Negra, R. Gearhart, J. J. Murray, P. Seyboth, C. K. Sinclair, I. O. Skillicorn, H. Spitzer, G. Wolf, H. H. Bingham, W. B. Fretter, W. J. Podolsky, M. S. Rabin, A. H. Rosenfeld, R. Windmolders, G. P. Yost and R. H. Milburn, Phys. Rev. D5, 1603 (1972).
8. K. C. Moffeit (private communication).
9. A. M. Boyarski, D. Coward, S. Ecklund, B. Richter, D. Sherden, R. Siemann and C. Sinclair, Contribution to the International Symposium On Electron and Photon Interactions at High Energy, Ithaca, New York (1971) and private communication.
10. For example, see C.F.A. Pantin, University of Cambridge, preprint no. DAMTP 7219 (1972).

TABLE I

$$\text{Partial multiplicities for } x_0 = 0.2: \frac{1}{\sigma(q^2, \nu)} \int_{x_0}^1 dx \int_0^\infty dp_\perp^2 \frac{d^2\sigma(q^2, \nu)}{dp_\perp^2 dx}$$

A)  $4 < \nu < 14$  GeV

$q^2$ [(GeV/c) <sup>2</sup> ]	$h^-$	$h^+$
-0.5 to -1.0	0.197 ± 0.007	0.312 ± 0.007
-1.0 to -1.5	0.211 ± 0.011	0.361 ± 0.015
-1.5 to -2.0	0.194 ± 0.016	0.384 ± 0.022
-2.0 to -2.5	0.221 ± 0.027	0.436 ± 0.035

B)  $-0.5 > q^2 > -2.5$  (GeV/c)<sup>2</sup>

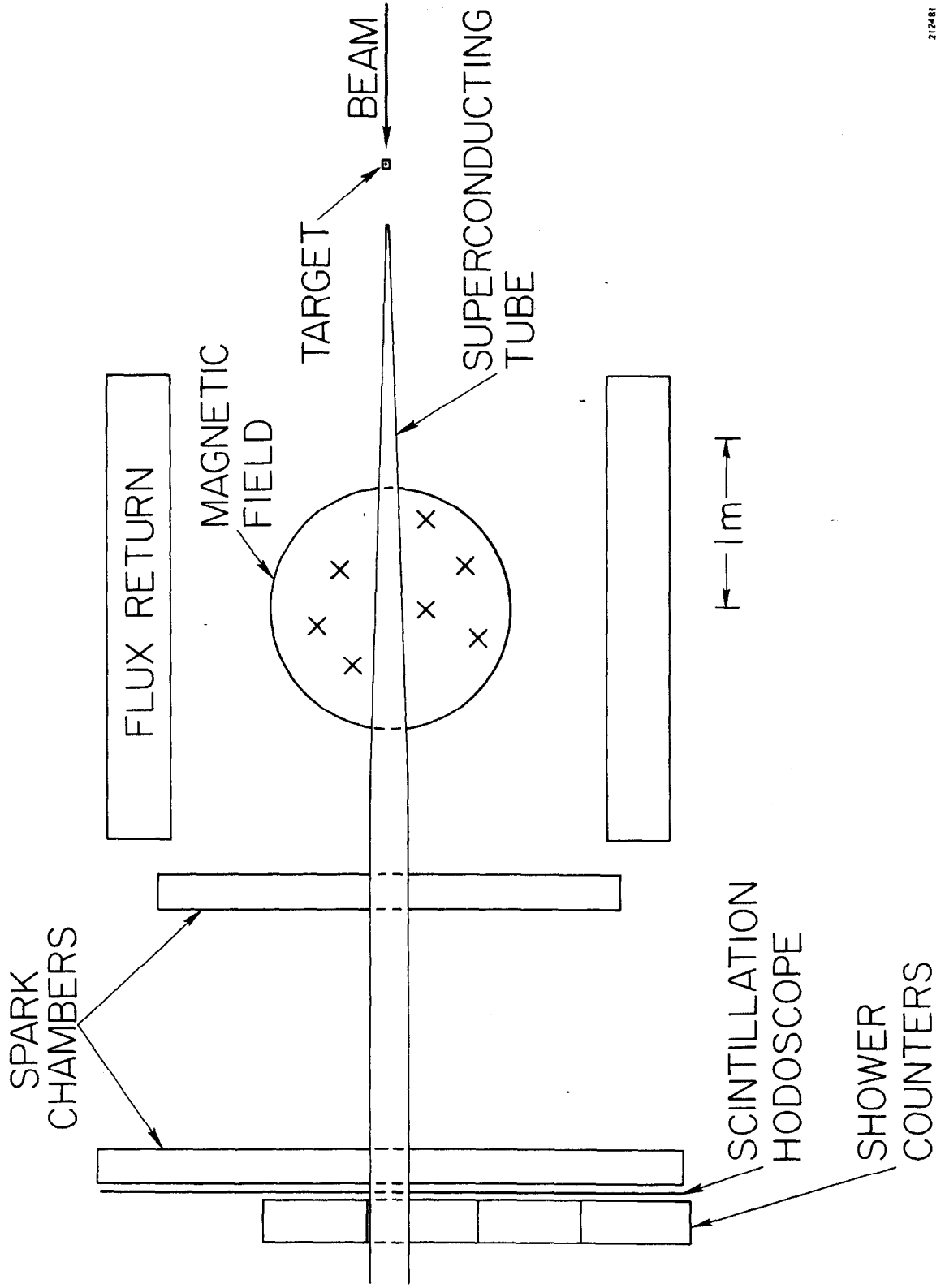
$\nu$ (GeV)	$h^-$	$h^+$
4.0 to 6.5	0.191 ± 0.011	0.398 ± 0.015
6.5 to 9.0	0.203 ± 0.010	0.353 ± 0.013
9.0 to 11.5	0.218 ± 0.011	0.334 ± 0.012
11.5 to 14.0	0.193 ± 0.011	0.301 ± 0.013

## FIGURE CAPTIONS

1. Schematic view of the apparatus.
2. Geometric acceptance of the apparatus averaged over the aximuthal angle.
3. Photograph of a typical  $\rho$ -like event.
4. Dependence of the invariant cross section on  $\varphi$ .
5. Dependence of the invariant cross section on  $p_{\perp}^2$  for  $-0.5 > q^2 > -2.5$ ,  $4 < \nu < 14$ . The lines are best fits of the form  $e^{-bp_{\perp}^2}$ , and are drawn in Figs. 6 and 7 also.
6. Dependence on  $p_{\perp}^2$  for negative hadrons in four  $q^2$  regions. The same line is drawn on all curves to aid in visual comparison.
7. Dependence on  $p_{\perp}^2$  for positive hadrons in four  $q^2$  regions. The same line is drawn on all curves to aid in visual comparison.
8. The slope parameters (b) taken from fits to the data in Figs. 6, 7. A point from  $\pi^-$  photoproduction (Ref. 7) is included.
9. Dependence of the invariant cross section on x for  $-0.5 > q^2 > -2.5$ ,  $4 < \nu < 14$ . A line representing the data in  $\pi^-$  photoproduction (Ref. 7) is included.
10. Dependence on x for negative hadrons in four  $q^2$  regions. The same line is drawn on all curves to aid in visual comparison.
11. Dependence on x for positive hadrons in four  $q^2$  regions. The same line is drawn on all curves to aid in visual comparison.
12. The ratio of the invariant cross section for positive to negative hadrons at each x for  $-0.5 > q^2 > -2.5$  and  $4 < \nu < 14$ .
13. The ratios of the invariant cross section for positive to negative hadrons at each  $q^2$  for two different x ranges. A point at  $q^2 = 0$  from photoproduction (Refs. 8 and 9) is included.

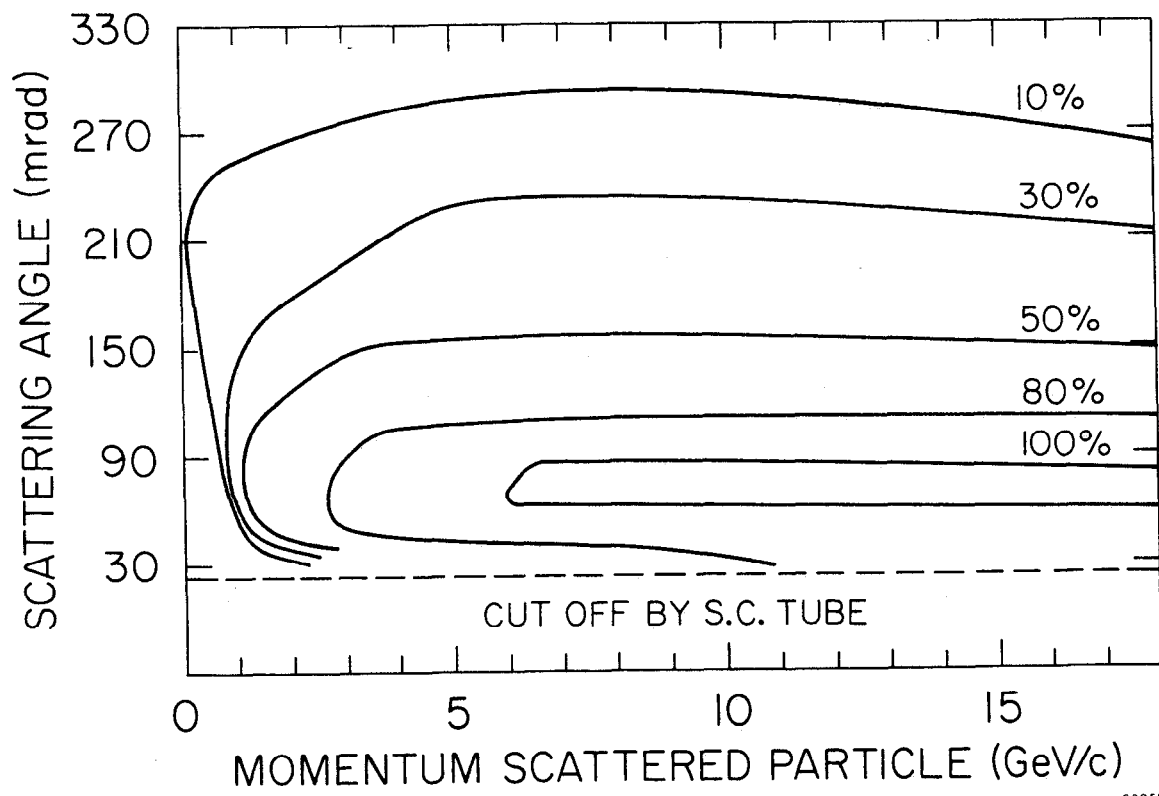
14. Sample mass distribution of events consistent with the hypothesis

$$\gamma^* p \rightarrow \pi^+ \pi^- p.$$



212481

FIG. 1



209581

FIG. 2

# TYPICAL "Rho" EVENT

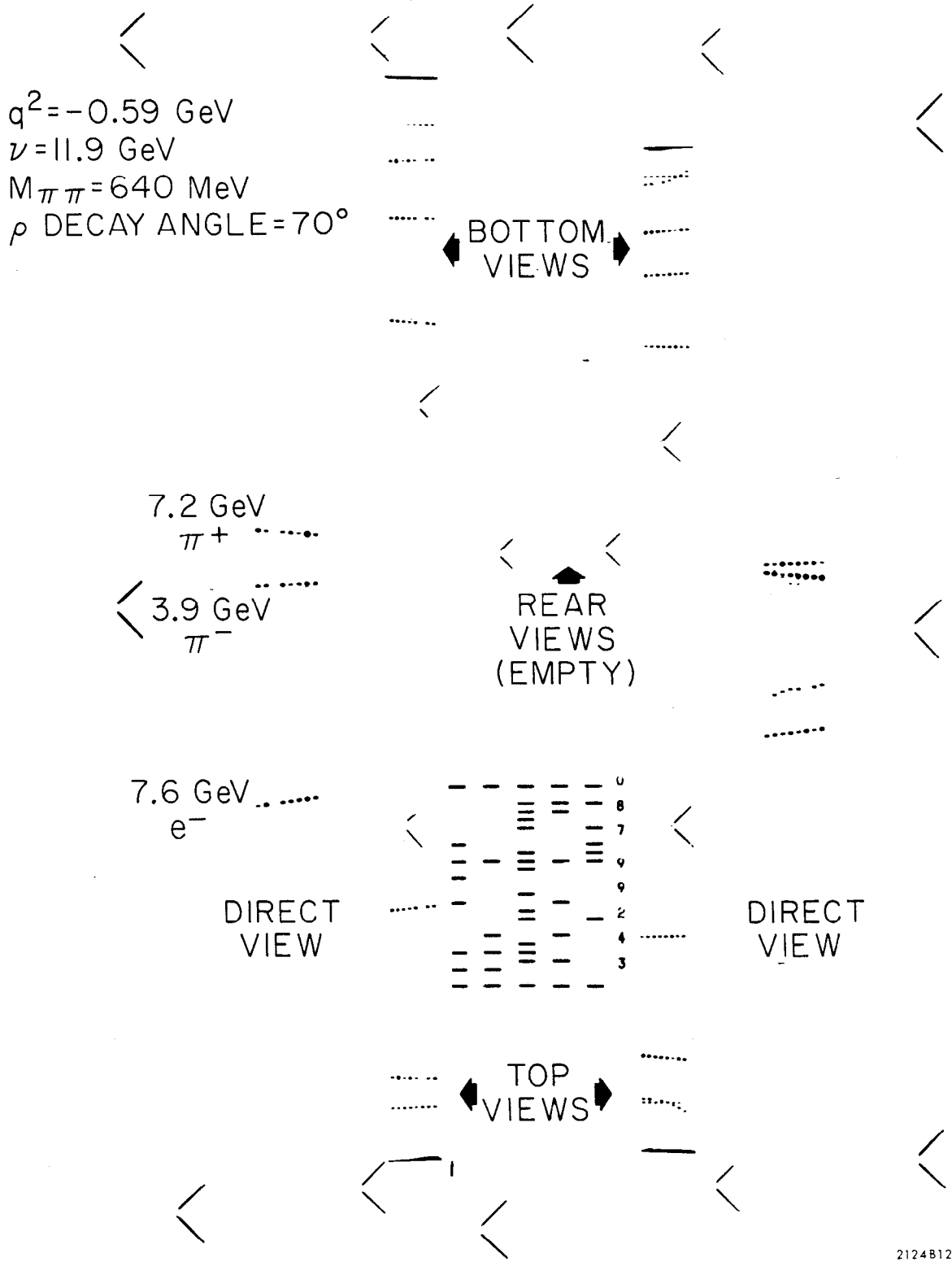
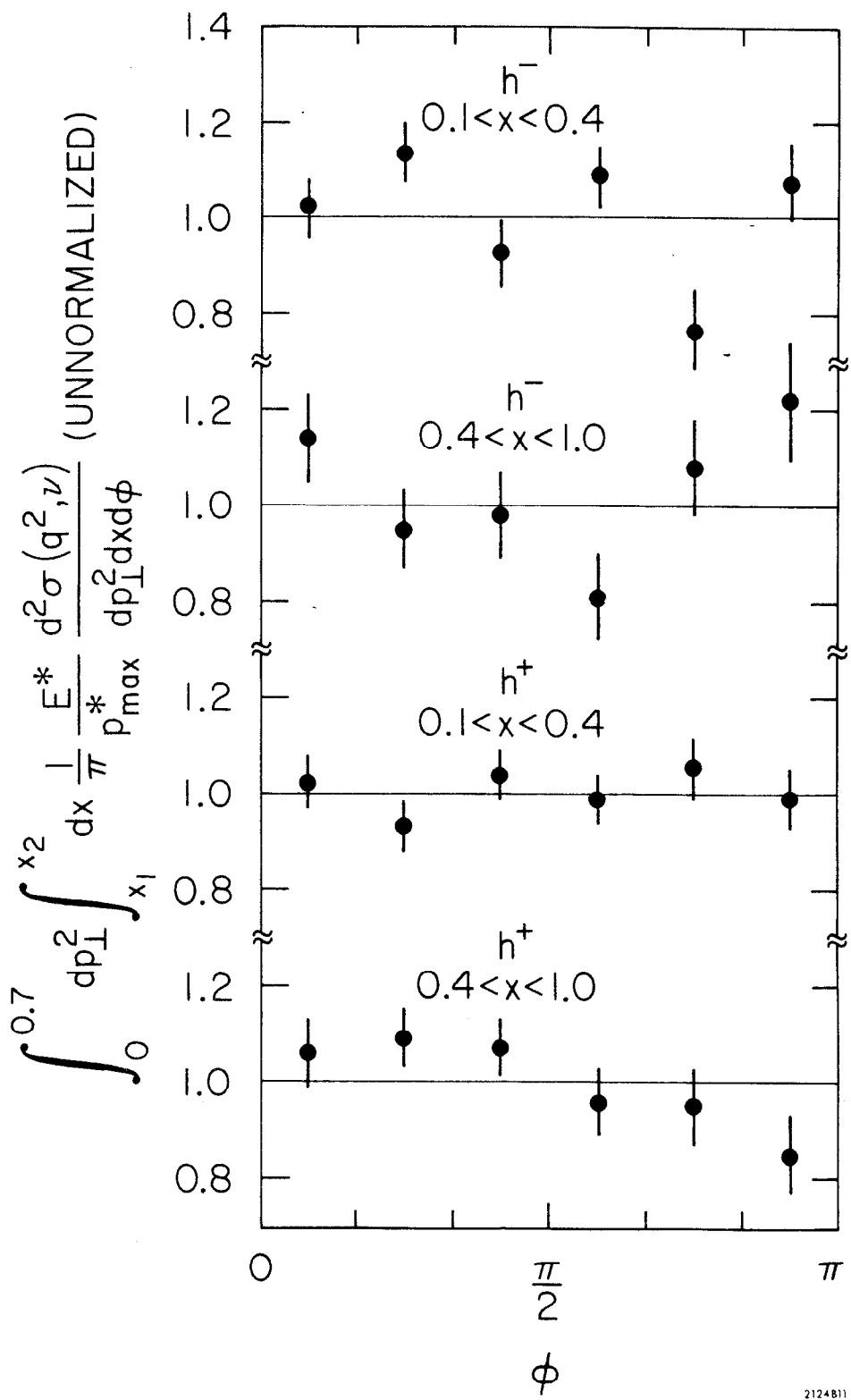


FIG. 3

PRELIMINARY  
 AZIMUTHAL DISTRIBUTION  
 $\gamma^*p \rightarrow h + (\text{ANYTHING})$

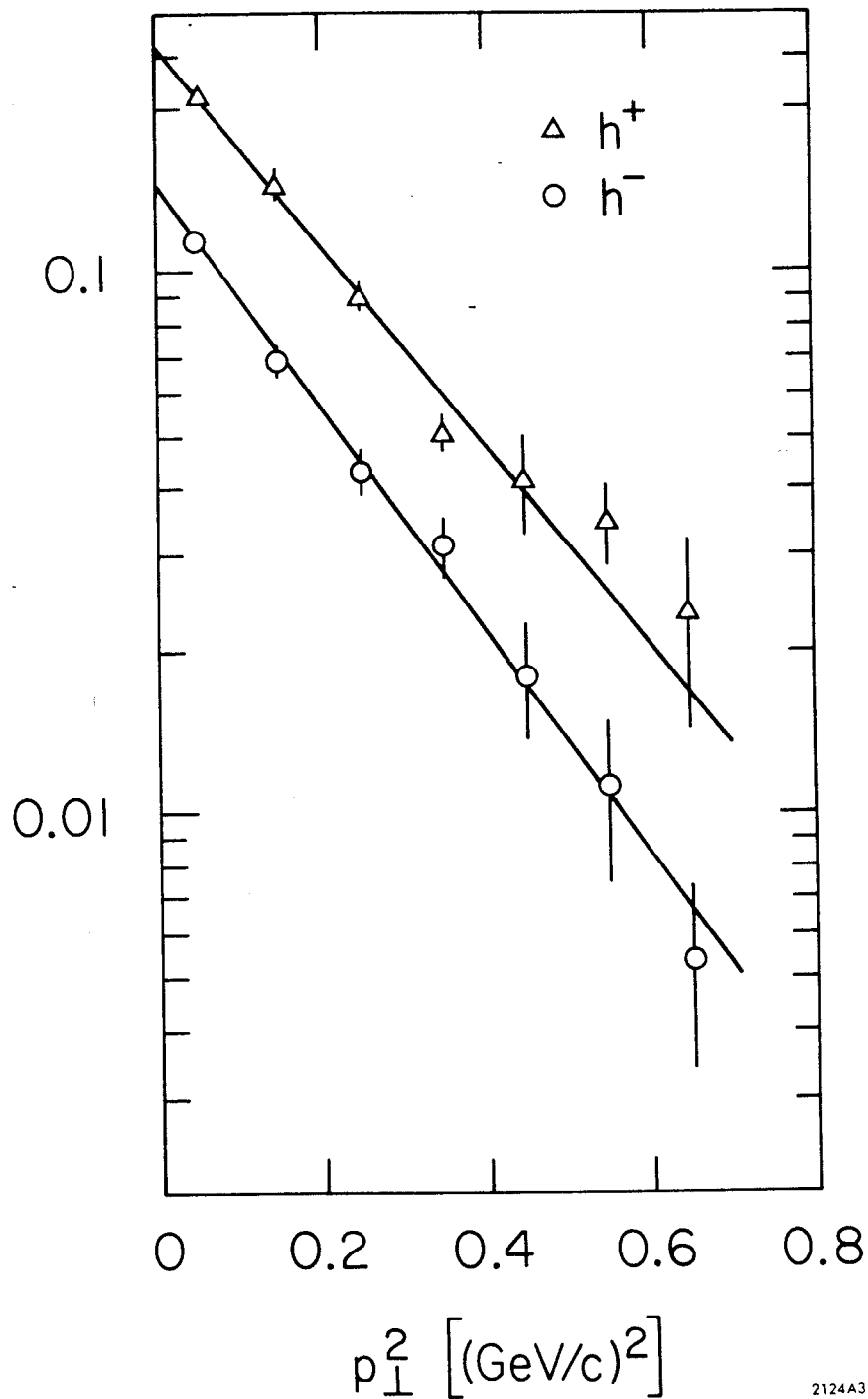


2124811

FIG. 4

PRELIMINARY  
 $\gamma^* p \rightarrow h + (\text{ANYTHING})$

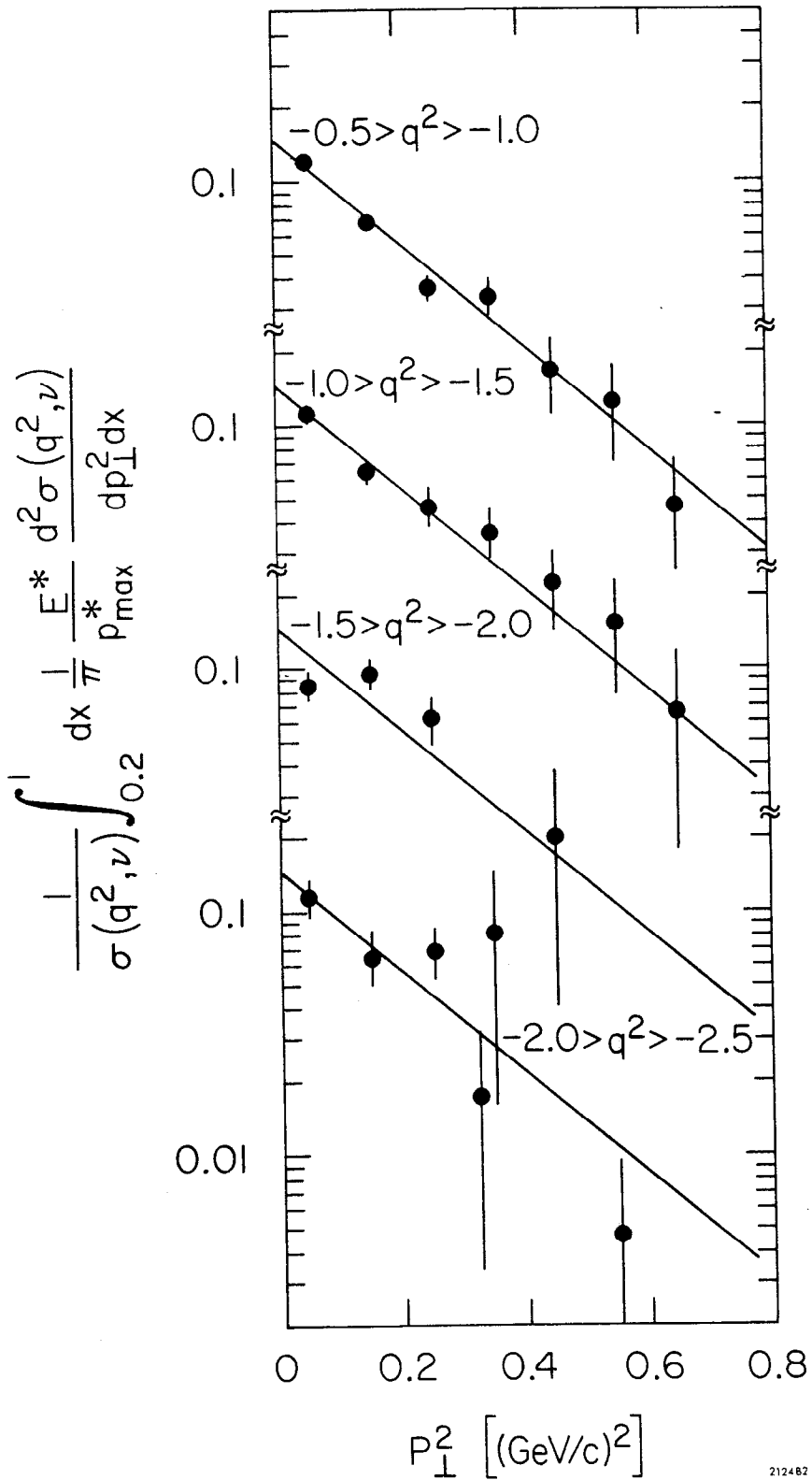
$$\frac{1}{\sigma(q^2, \nu)} \int_0^1 dx \frac{1}{\pi} \frac{E^*}{p_{\text{max}}^*} \frac{d^2 \sigma(q^2, \nu)}{dp_{\perp}^2 dx}$$



2124A3

FIG. 5

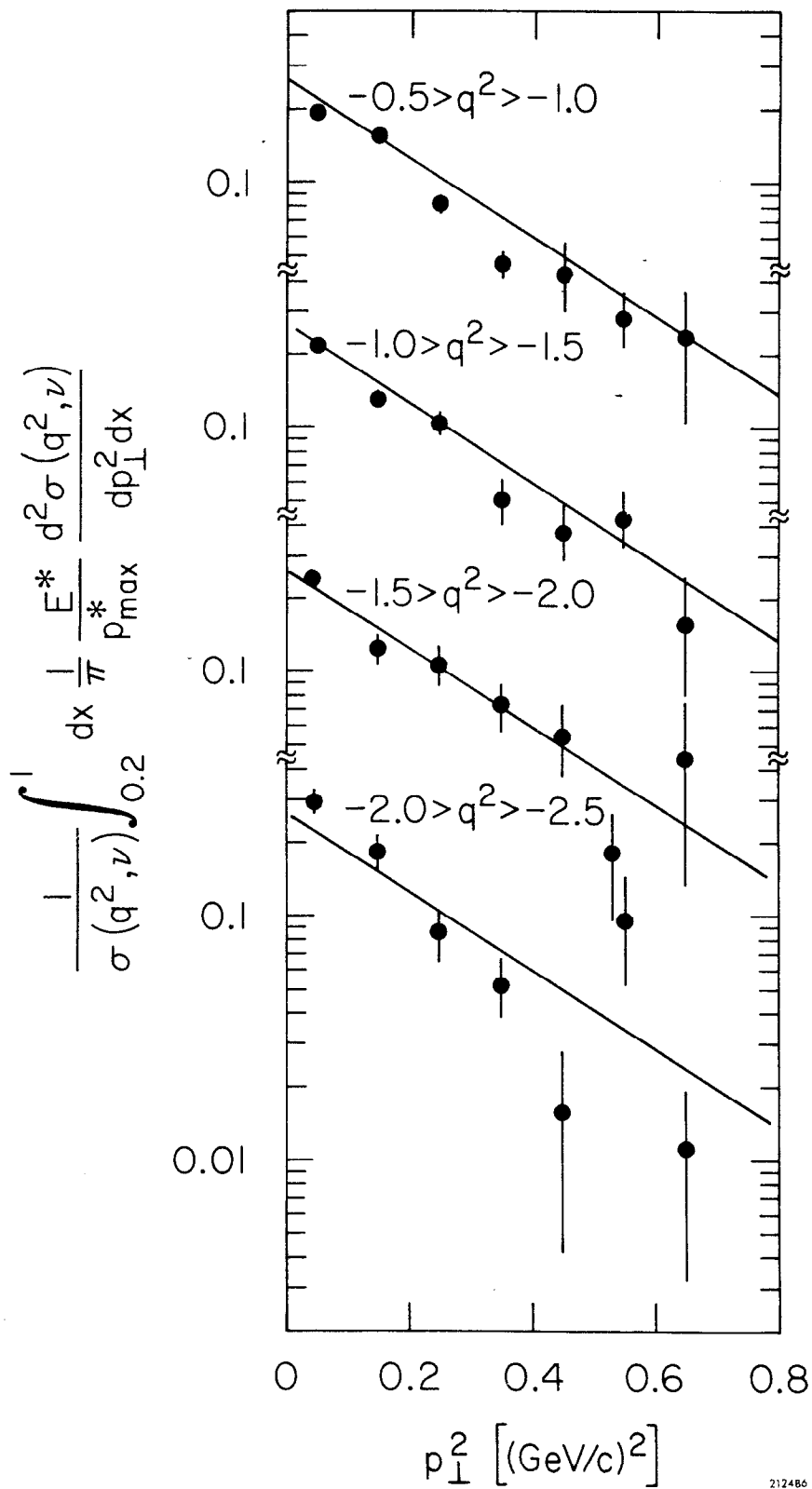
PRELIMINARY  
 $\gamma^* p \rightarrow h^- + (\text{ANYTHING})$



212482

FIG. 6

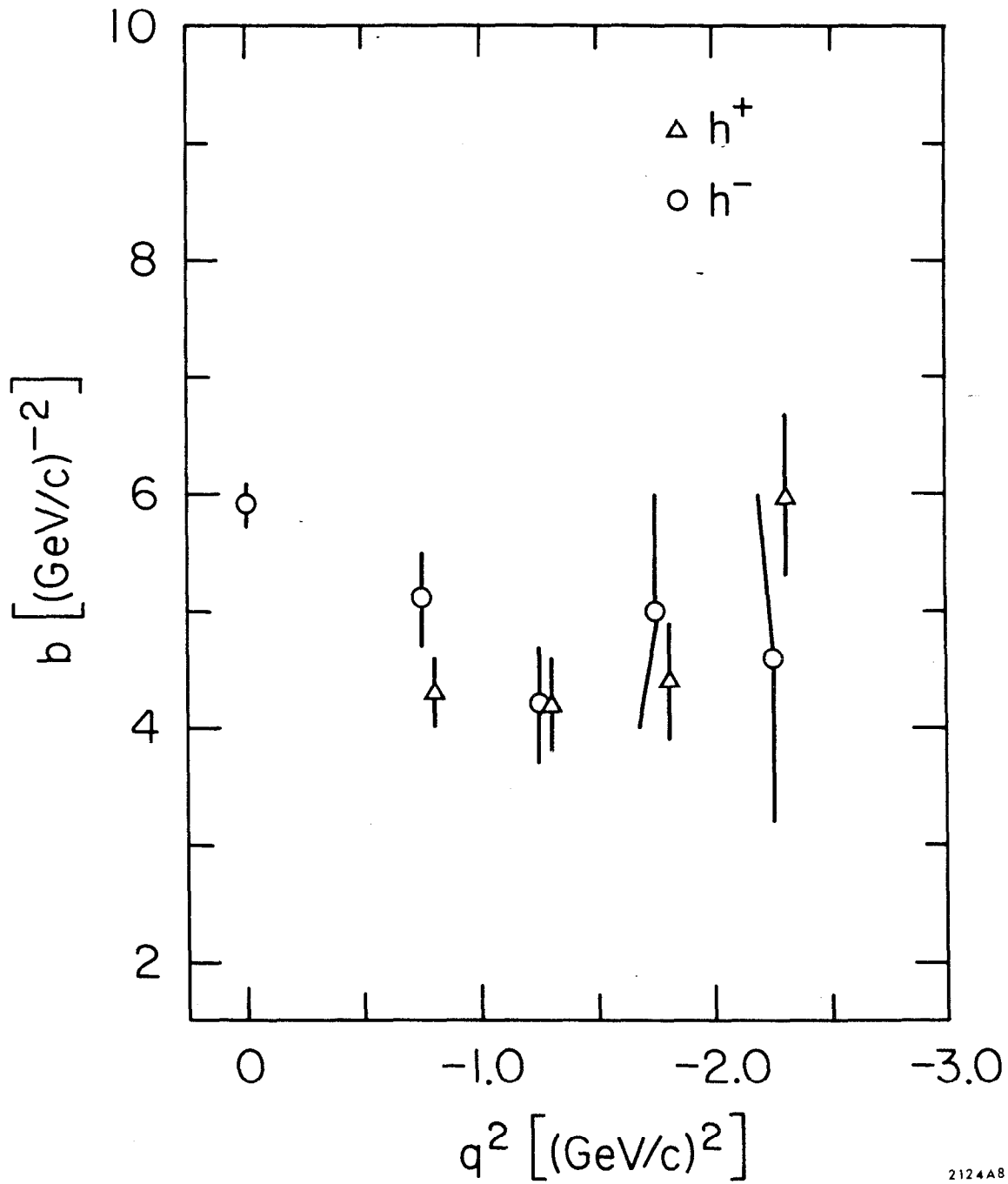
PRELIMINARY  
 $\gamma^*p \rightarrow h^+ + (\text{ANYTHING})$



212486

FIG. 7

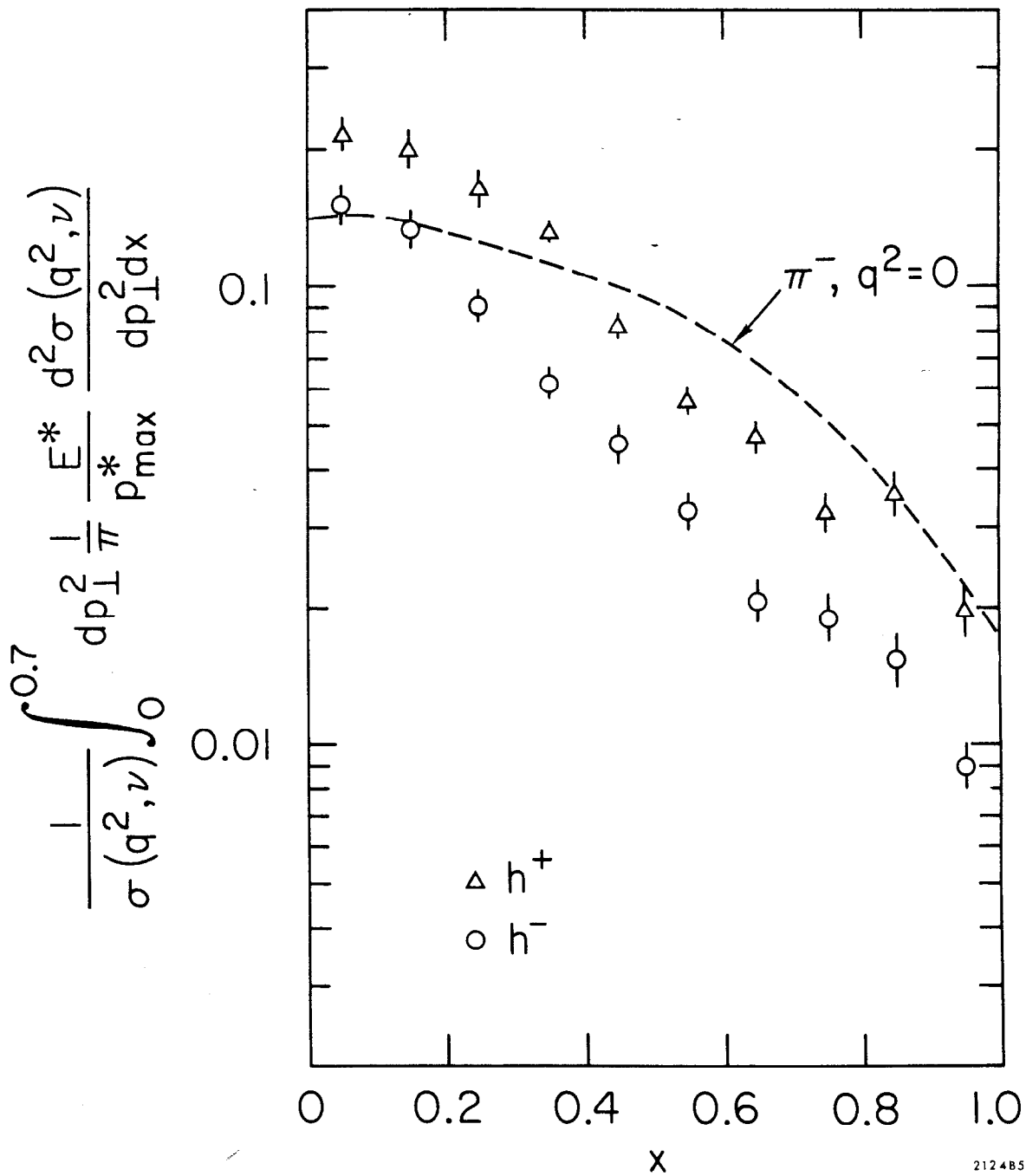
PRELIMINARY  
 $\gamma^*p \rightarrow h + (\text{ANYTHING})$   
FIT TO  $\Delta e^{-bp_{\perp}^2}$



2124A8

FIG. 8

PRELIMINARY  
 $\gamma^* p \rightarrow h^- + (\text{ANYTHING})$   
 $-0.5 > q^2 > -2.5$



212485

FIG. 9

PRELIMINARY  
 $\gamma^*p \rightarrow h^- + (\text{ANYTHING})$

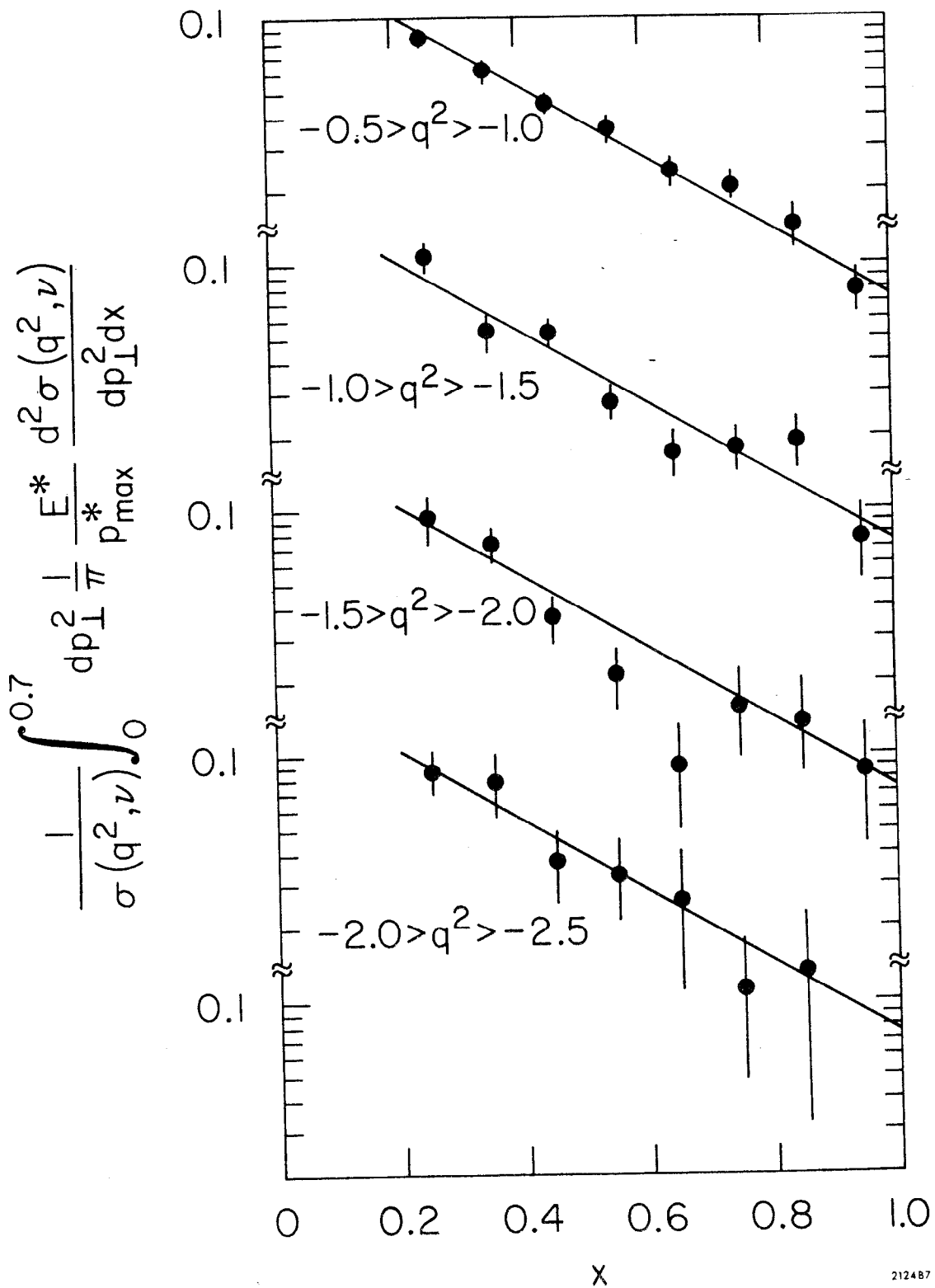
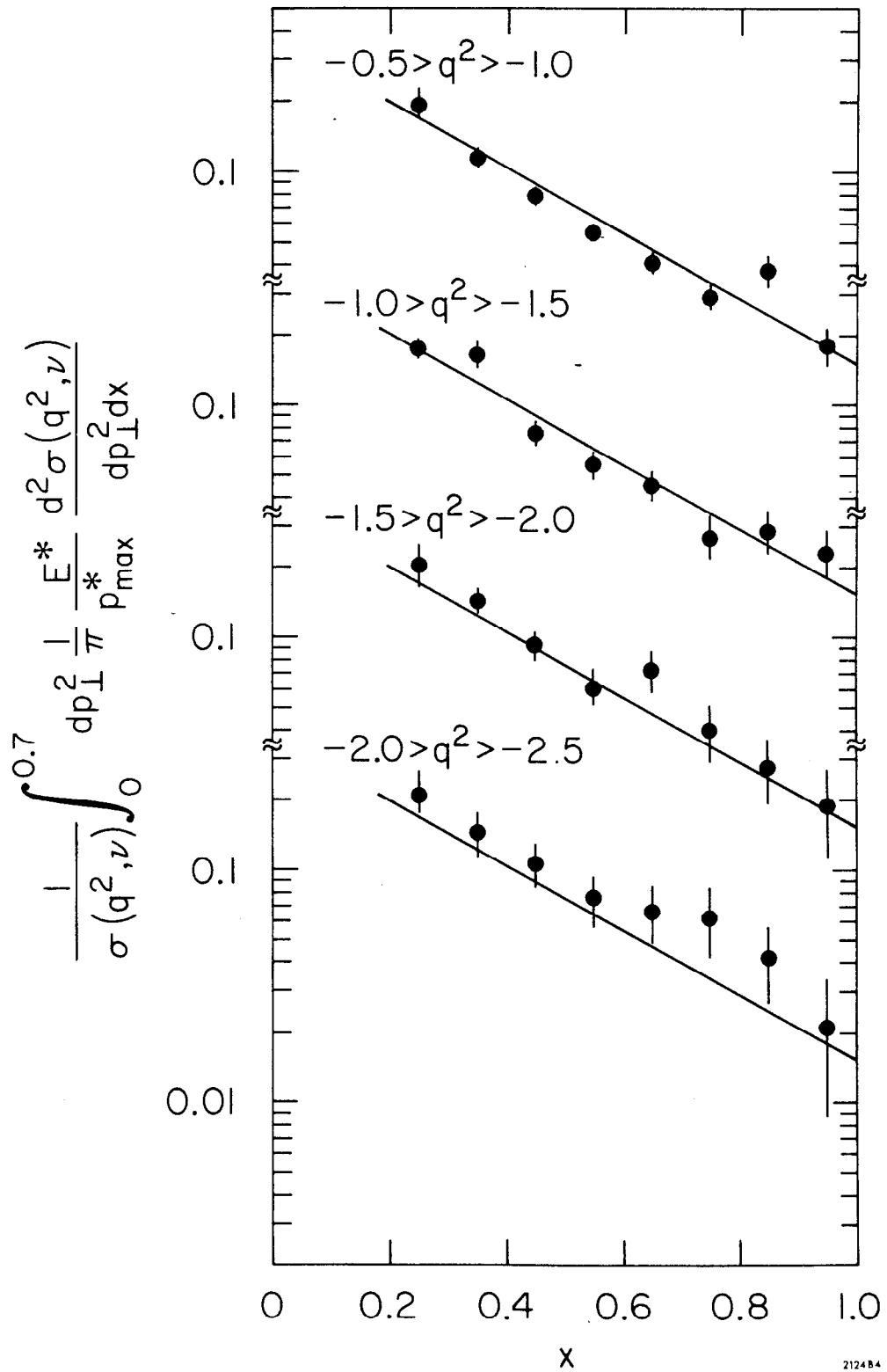


FIG. 10

PRELIMINARY  
 $\gamma^*p \rightarrow h^+ + (\text{ANYTHING})$



2124B4

FIG. 11

PRELIMINARY  
 $\gamma^* p \rightarrow h + (\text{ANYTHING})$   
CHARGE RATIO

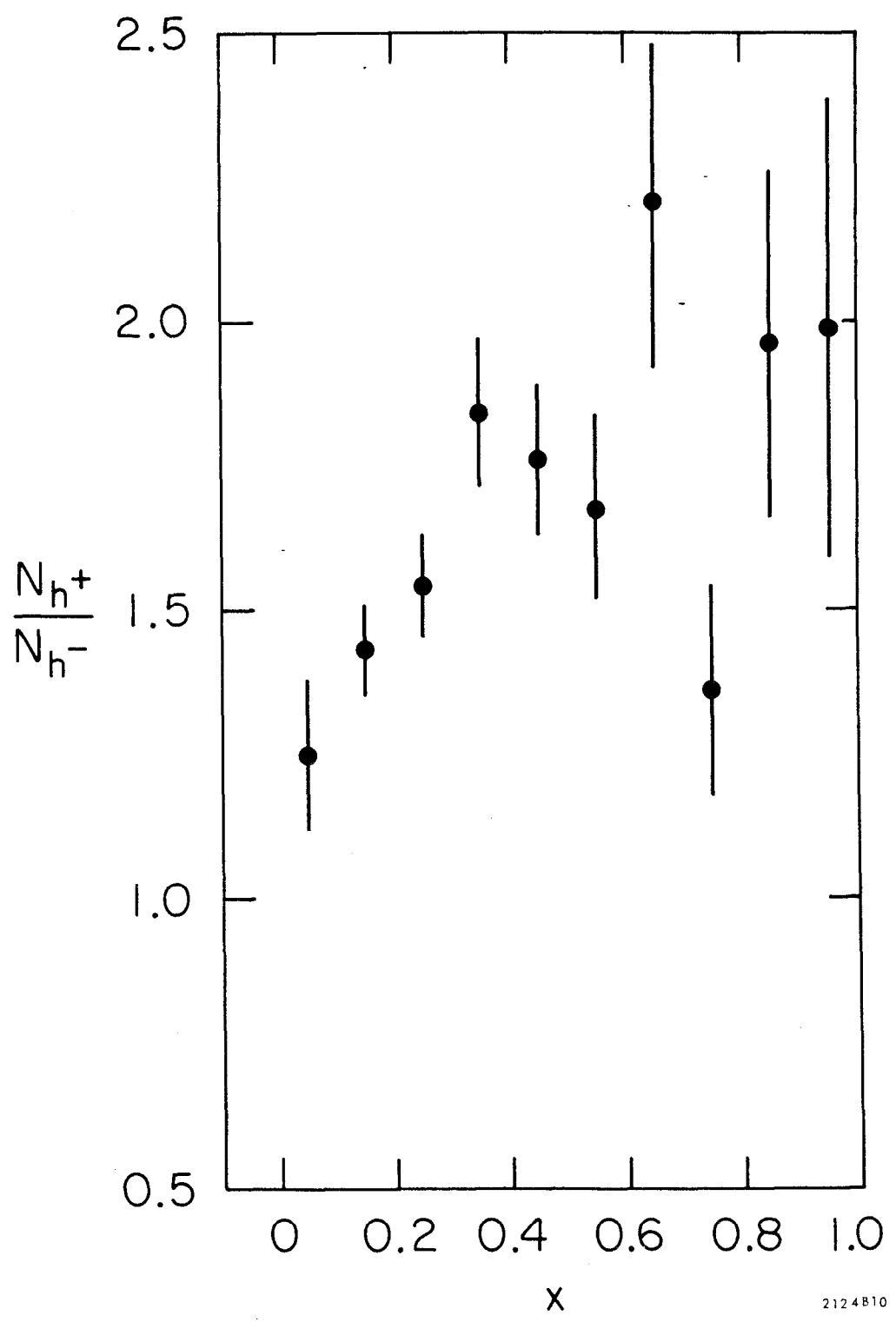


FIG. 12

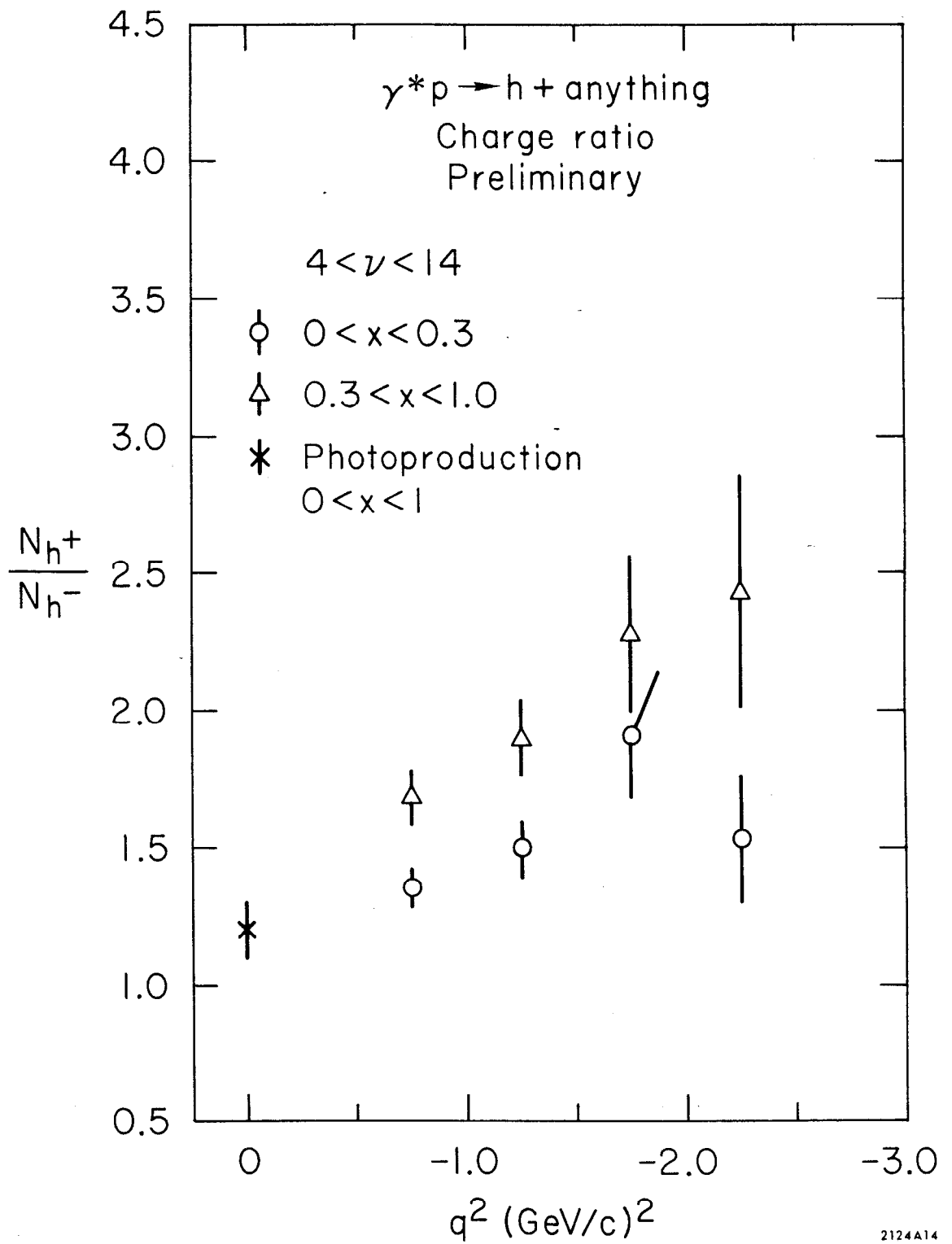


FIG. 13

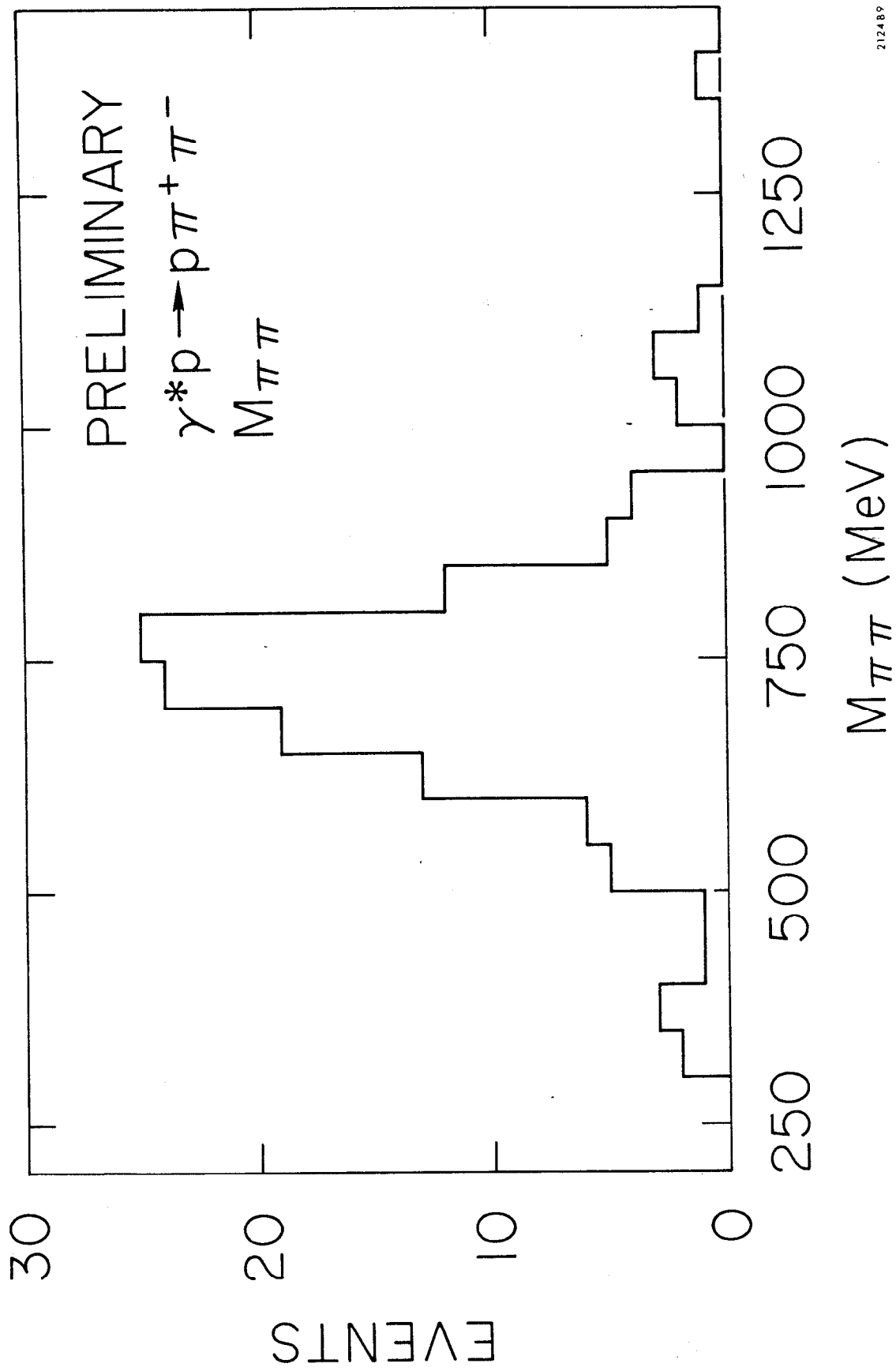


FIG. 14